

# Temperature effect on seismic performance of CBFs equipped with SMA braces

Canxing Qiu\* and Xingnan Zhao<sup>a</sup>

School of Civil Engineering, Shandong University, Jinan, 250061, China

(Received July 5, 2018, Revised October 6, 2018, Accepted October 16, 2018)

**Abstract.** Shape memory alloys (SMAs) exhibit superelasticity given the ambient temperature is above the austenite finish temperature threshold, the magnitude of which significantly depends on the metal ingredients though. For the monocrystalline CuAlBe SMAs, their superelasticity was found being maintained even when the ambient temperature is down to  $-40^{\circ}\text{C}$ . Thus this makes such SMAs particularly favorable for outdoor seismic applications, such as the framed structures located in cold regions with substantial temperature oscillation. Due to the thermo-mechanical coupling mechanism, the hysteretic properties of SMAs vary with temperature change, primarily including altered material strength and different damping. Thus, this study adopted the monocrystalline CuAlBe SMAs as the kernel component of the SMA braces. To quantify the seismic response characteristics at various temperatures, a wide temperature range from  $-40$  to  $40^{\circ}\text{C}$  are considered. The middle temperature,  $0^{\circ}\text{C}$ , is artificially selected to be the reference temperature in the performance comparisons, as well the corresponding material properties are used in the seismic design procedure. Both single-degree-of-freedom systems and a six-story braced frame were numerically analyzed by subjecting them to a suite of earthquake ground motions corresponding to the design basis hazard level. To the frame structures, the analytical results show that temperature variation generates minor influence on deformation and energy demands, whereas low temperatures help to reduce acceleration demands. Further, attributed to the excellent superelasticity of the monocrystalline CuAlBe SMAs, the frames successfully maintain recentering capability without leaving residual deformation upon considered earthquakes, even when the temperature is down to  $-40^{\circ}\text{C}$ .

**Keywords:** shape memory alloy; temperature effect; braced frame; seismic performance; numerical analysis

## 1. Introduction

Shape memory alloys (SMAs) are a class of alloys which are able to recover large deformation through heating (*shape memory effect*) or unloading (*superelastic effect*) (Song *et al.* 2006, Qiu *et al.* 2018a). The superelastic property are particularly favored by the earthquake engineering community, because SMAs promptly recover large deformation without requiring external heating treatment during the attenuation of ground shakings. In addition, most SMAs have satisfactory damping behavior, high fatigue life and good machinability. Therefore, exploring SMAs emerges as a promising strategy to assist the deformed structures to immediately return to their at-rest positions after earthquakes. Past decades have evidenced the remarkable achievement in applying SMAs to develop various types of seismically resilient structures from both the component and system levels (Park and Park 2016, Katariya *et al.* 2017, Zhu and Zhang 2008, Qiu and Zhu 2017, Ozbulut and Silwal 2016, Torra *et al.* 2014, Liu *et al.* 2011, Fang *et al.* 2014, Casciati and Faravelli 2009), through the manner of controlling peak deformation and

reducing residual deformation.

Among the efforts over past years, SMA braces (SMABs) were particularly developed to solve the problems associated with concentrically braced frames (CBFs) equipped with conventional braces or/and buckling-restrained braces (BRBs). The corresponding frame, i.e. SMA braced frames (SMABFs) gained wide attentions. Belonging to non-buckling braces, SMABs not only successfully conquer the buckling induced instability problem for conventional braces (Sabelli *et al.* 2003), but also well addressed the unrecoverable deformation of BRBs (Zhu and Zhang 2008, Fahnestock *et al.* 2007, Kiggins and Uang 2006). More importantly, upon design basis earthquakes (DBE), the residual interstory drift ratios of CBFs with BRBs may exceed 0.5%, which represents the threshold of demolishing the inclined buildings, instead of repairing them (McCormick *et al.* 2008). Therefore, although collapses can be prevented by installing existing braces, excessive residual deformation still leads to direct socio-economic loss after earthquakes. Promising results on the studies of SMABs were reported based on experimental or numerical analyses in recent years. Qiu and Zhu (2017) observed desirable seismic performance of SMABFs upon far- and near- field earthquakes though a series of shake table tests. McCormick *et al.* (2007) demonstrated that SMABs are superior to conventional steel braces in controlling both peak and residual deformations for CBFs. Zhu and Zhang (2008) and Qiu *et al.* (2018a) showed that SMABs and BRBs are able to control peak deformation

\*Corresponding author, Assistant Professor

E-mail: [qiucanxing@sdu.edu.cn](mailto:qiucanxing@sdu.edu.cn)

<sup>a</sup> Master student

E-mail: [ZhaoXNan@yeah.net](mailto:ZhaoXNan@yeah.net)

within comparable level, whereas the former eliminated residual deformation at the mean time.

It should be noted that SMAs are relatively sensitive to temperature variation, due to the intrinsic thermo-mechanical coupling mechanism (Qiu and Zhu 2014), compared to the other conventional materials in civil engineering. However, this characteristic was seldom taken into account by prior seismic studies so far. In either experimental tests or numerical analyses, the effect of temperature variation was usually excluded by assuming the framed structures are working in an environment with high and stable temperature. Although people noticed this problem, most of them paid attention on bridges (Andrawes and DesRoches 2007, Zhang *et al.* 2010, Ozbulut and Hurlebaus 2010). In fact, besides with the applications of SMAs in bridges, the installed SMA-based braces or dampers in building structures are also possible to operate in an outdoor environment and are likely to endure temperature variation, since the effect of ambient temperature on structures also raises concerns during earthquakes (Ozbulut and Hurlebaus 2012, Chang *et al.* 1992, Chang *et al.* 1995, Tsai 1994, Guo *et al.* 2016).

However, to the best knowledge of the authors, the effect of temperature variation on the seismic behavior of SMABFs is yet to be known. Therefore, this study aims to address this issue for multi-story SMABFs that are exposed to severe temperature oscillations. In this study, the monocrystalline CuAlBe SMA (Qiu and Zhu 2014, Torra *et al.* 2010) is selected attributed to the large recentering strain and very wide operating temperature, which actually distinguishes them from other known SMAs. To evaluate the effect of temperature variation, 0°C is denoted as the reference temperature, and the interested temperature range is from -40 to 40°C with an interval of 20°C. In this study, the effect of temperature variation was firstly assessed on flag-shape (FS) single-degree-of-freedom (SDOF) systems that represent the global behavior of the SMABFs. Later, this paper designed a six-story SMABF at the reference temperature, and then assessed the seismic performance at the other temperatures. The input earthquake ground motion records are corresponding to the DBE seismic hazard level.

## 2. Monocrystalline CuAlBe SMA

Upon earthquakes, SMAs will endure a number of cyclic loading strains, which requires a high ductility capacity. In addition, the deformation of SMAs activates the phase transformation between different crystals, whereas the sensitivity to temperature variation depends on material compositions. According to the studies (Qiu and Zhu 2014, Zhang *et al.* 2008), the ductility capacity of polycrystalline CuAlBe SMAs is fairly limited from the perspective of seismic applications. The NiTi SMAs, which currently attract the most attention in earthquake engineering (Song and Ma 2006, DesRoches and Smith 2004, Ozbulut *et al.* 2011, Araki *et al.* 2011), start to lose superelasticity at 0°C and are completely unrecoverable at -25°C (Zhang *et al.* 2010), and show relatively higher sensitivity to temperature variation than the copper-based SMAs (Zhang *et al.* 2010),

thus are not appropriate for outdoor applications. Therefore, the monocrystalline CuAlBe SMAs are adopted in this study, because they combine the merits of these two types of SMAs. More discussions on CuAlBe SMAs can be found in related studies (de Castro *et al.* 2013, Sade *et al.* 2014).

Currently adopted CuAlBe was tested by a prior study (Qiu and Zhu 2014). As reported, this CuAlBe was obtained from NIMESIS Technology Inc. The chemical composition in terms of weight is close to Cu≈87%, Al≈12% and Be=0.45-0.68%. The cyclic loading results of monocrystalline CuAlBe SMA wires at various ambient temperatures can be found in the corresponding study (Qiu and Zhu 2014). The elastic modulus in austenite state,  $E_A$ , is almost insensitive to temperature variation and is assumed to be constantly 17 GPa. The strength capacity increased linearly with the increment of ambient temperature at a rate of 1.38 MPa/°C by curve fitting analysis, as shown in Fig. 1. The temperature effect is inherent to the martensitic transformation of the SMA. The second law of thermodynamics establishes the existence of a Clausius-Clapeyron equation that links the stress with the temperature. The stress to transform at a given temperature depends also on the orientation. Usually, the orientation of the single crystal axes can be determined by the X-Ray Laue method. However, due to the lack of device, the authors are currently not able to provide this information to readers. The hysteretic characteristics, i.e. the 'post-yield' stiffness and hysteresis width, are almost unaffected by temperature variation. This FS approximation to the actual force-deformation relationship of SMAs has been adopted and verified by previous studies (Qiu and Zhu 2017, Zhu and Zhang 2013). The interested hysteretic parameters are expressed below as a function of temperature,  $T$ :

$$\sigma_{Ms} = 1.38T + 139 \quad (1)$$

$$\sigma_{Af} = 1.38T + 89 \quad (2)$$

$$\varepsilon_{Ms} = \sigma_{Ms} / E_A \quad (3)$$

$$\beta = (\sigma_{Ms} - \sigma_{Af}) / \sigma_{Ms} \quad (4)$$

$$\zeta_{eq} = E_D / (4\pi E_{So}) \quad (5)$$

where  $\sigma_{Ms}$  and  $\sigma_{Af}$  are the stresses corresponding to the start of forward phase transformation and finish of backward phase transformation;  $\varepsilon_{Ms}$  is the strain associated with forward phase transformation.  $\beta$  is a parameter that characterizes the hysteresis shape of SMAs.  $\zeta_{eq}$  is the equivalent damping ratio (Chopra 1995), which depends on the area  $E_D$  enclosed by the hysteresis loop and the strain energy  $E_{So}$ , as shown in Fig. 2. The parameters of  $\sigma_{Ms}$  and  $\varepsilon_{Ms}$  mimic the yield stress and strain of steels, respectively.

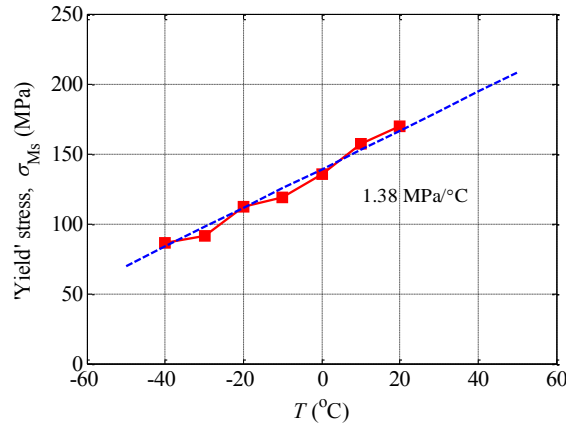


Fig. 1 'Yield' stress-temperature relationship of the monocrystalline CuAlBe

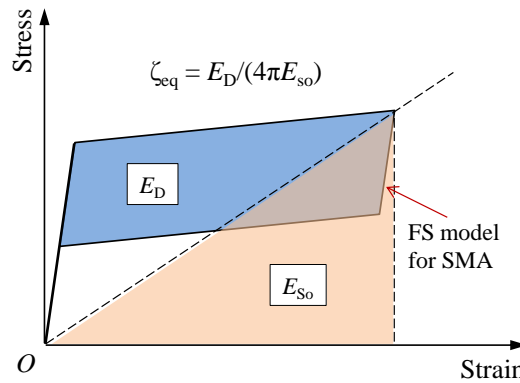


Fig. 2 Flag-shape model for SMA and definition of equivalent damping ratio for SMA

Table 1 Hysteretic parameters of monocrystalline CuAlBe SMAs

Temperature (°C)	$\sigma_{Ms}$ (MPa)	$\sigma_{Af}$ (MPa)	$\epsilon_{Ms}$ (%)	$E_A$ (GPa)	$\alpha$	$\beta$	$\zeta_{eq}$ (%)*
-40	83.8	33.8	0.49	17	0.03	0.60	11.9
-20	111.4	61.4	0.66			0.45	8.8
0	139.0	89.0	0.82			0.36	7.0
20	166.6	116.6	0.98			0.30	5.9
40	194.2	144.2	1.14			0.26	5.2

\* corresponding to the strain of 0.11

The hysteretic parameters at various environmental temperatures are listed in Table 1.  $\alpha$  is a parameter measuring the 'post-yield' stiffness ratio. It is seen that when the temperature is decreased from 40 to  $-40^\circ\text{C}$ , the strength is decreased from 194.2 to 83.8 MPa, whereas the value of  $\beta$  increases from 0.26 to 0.60, and the equivalent damping ratio is increased from 5.2% to 11.9%. Therefore, it is worth noting that the combined effect of strength capacity and hysteresis width leads to an increased equivalent damping ratio at low temperature, which may bring about benefits to seismic response because a large damping is usually beneficial to vibration control. Parenthetically, for the adopted monocrystalline CuAlBe, its hysteresis width is relatively narrow, compared with most polycrystalline

CuAlBe. Considering the hysteresis width directly determines the damping capacity, the structural deformation can be thus reduced when polycrystalline CuAlBe is used.

### 3. SMAB

Various configurations of SMABs were proposed in past years (Zhu and Zhang 2008, Qiu and Zhu 2017). This study adopted a possible configuration from the study (Qiu and Zhu 2017), as shown in Fig. 3. Compared to its counterparts, the selected configuration solely utilizes superelastic SMA cables, instead of cooperating additional damping source. Thus, the behavior of such SMAB is entirely dependent on

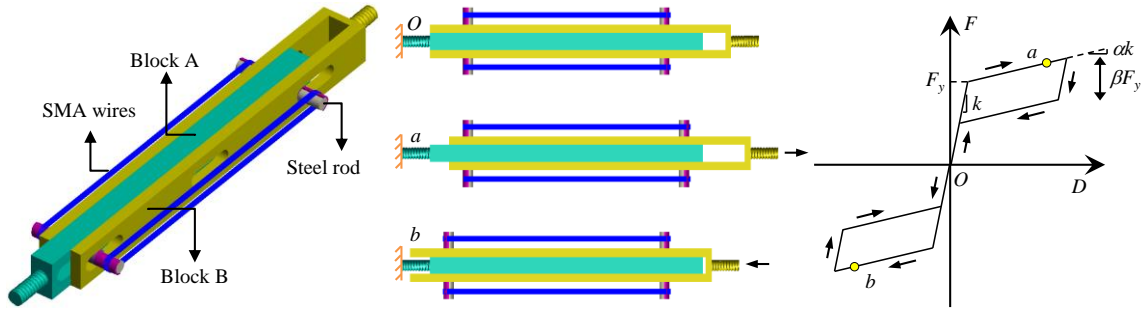


Fig. 3 Configuration and working principle of the SMAB (Qiu and Zhu 2017)

the properties of installed SMAs. The brace consists of a SMA-based damper and two rigid steel square tubes at both ends. The monocrystalline CuAlBe SMA cables are wrapped on the steel rods, which move in the slots and elongate the cables. Through the proposed working mechanism, the SMA cables are always stretched, no matter the brace is subjected to tension or compression. Except for the SMA cables, all the other parts are sized by capacity design, with the aims to keep elastic and to avoid excessive deformation. Consequently, the input deformation is totally absorbed by the SMA cables. Such a configuration permits a convenient scalability of strength and stiffness of the adopted SMAB, given the total cross-sectional area and effective length of SMA cables are known.

**4. Ground motions**

Ground motions corresponding to the DBE seismic hazard level are selected in this study. A total of 20 records, designated as LA01–LA20, which were developed for Los Angeles by Somerville *et al.* (1997) are included currently. This suite of ground motions was widely used by many prior studies (Qiu and Zhang 2008, Qiu *et al.* 2018a, Qiu *et al.* 2018b, Hou *et al.* 2017, Qiu *et al.* 2017). To meet the DBE spectrum for this site, the original historical records were adjusted in their frequency domain, the soil type was also modified, and their amplitudes were properly scaled to match a 10% probability of exceedence in a 50-year period.

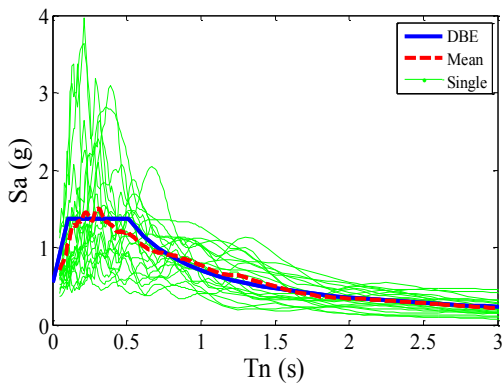


Fig. 4 Selected earthquake ground motion records

Fig. 4 plots the response spectra of each single ground motion record and the target design spectrum. Well agreement can be found between the mean response spectrum and the design spectrum over the entire period range, although discernible difference is noticed in the range of short periods. Noticeable deviation can be observed between each individual response spectrum, due to the uncertainty nature of earthquakes.

**5. SDOF systems**

Seismic analyses on SDOF systems that represent the global behavior of SMABFs were firstly conducted, prior to the analyses on multi-degree-of-freedom (MDOF) system, which refers to the multi-story frame in this study. As shown in Fig. 5, the strength reduction factor (Chopra and Goel 2002), *R*, is introduced to measure the strength capacity of the inelastic system, as a fraction of the strength of the corresponding elastic system. According to the definition, it is implied that varying environmental temperature essentially affects the strength reduction factor. The higher the temperature is, the smaller the *R* value will be. The SDOF structures, schematically shown in Fig. 6, are assumed to have a fundamental period of  $T_n = 1.1s$  and a strength reduction factor of 4 at the reference temperature. The SDOF analyses were conducted in MATLAB (2011). Newmark's method was used in the numerical calculations (Newmark 1959). The equation of motion for the SDOF system is given as

$$m\ddot{x} + c\dot{x} + F(x, \dot{x}) = -m\ddot{x}_g \tag{6}$$

where  $F(x, \dot{x})$  refers to the FS hysteresis behavior which describes the constitutive model of SMAs. The FS model is an approximate model for the real behavior of SMA (stress-strain at a given temperature). This could carry some margin over a real experiment because many real stress-strain cycles of pseudoelastic SMA's are not exactly rhomboidal. However, the idea of using a FS model to describe the reversible phase transformation processes of SMAs has been validated by previous studies (Qiu and Zhu 2017, Zhu and Zhang 2013). The FS constitutive model is schematically shown in Fig. 2. It is noted that  $F(x, \dot{x})$  depends on the ambient temperature.

In the SDOF analyses, the interested seismic performance indices include: the maximum displacement  $x_{\max}$ , the maximum acceleration  $a_{\max}$ , the normalized maximum absorbed energy  $E_{\text{abs}}$ , and the normalized maximum input energy  $E_{\text{input}}$ . The corresponding definitions are given as below

$$x_{\max} = \max_{0 \leq t \leq t_D} |x(t)| \quad (7)$$

$$a_{\max} = \max_{0 \leq t \leq t_D} |\ddot{x}(t) + \ddot{x}_g(t)| \quad (8)$$

$$E_{\text{abs}} = \max_{0 \leq t \leq t_D} \left| \int_0^{x(t)} F(x, \dot{x}) dx \right| / w \quad (9)$$

$$E_{\text{input}} = \max_{0 \leq t \leq t_D} \left| - \int_0^{x(t)} m \ddot{u}_g(t) dx \right| / w \quad (10)$$

where  $t_D$  is the total time duration of the earthquake.  $w$  is the building weight.  $x_{\max}$  is usually deemed as the a straightforward index that measures the damage degree of both structural and non-structural components (Moehle 1992).  $a_{\max}$  is closely related to the damage states of acceleration-sensitive non-structural components, and it directly determines the sustained strength demand of the SDOF systems during earthquakes.  $E_{\text{abs}}$  establishes the level of damage induced by earthquakes as well.  $E_{\text{input}}$  refers to imparted energy into the structures during earthquakes.

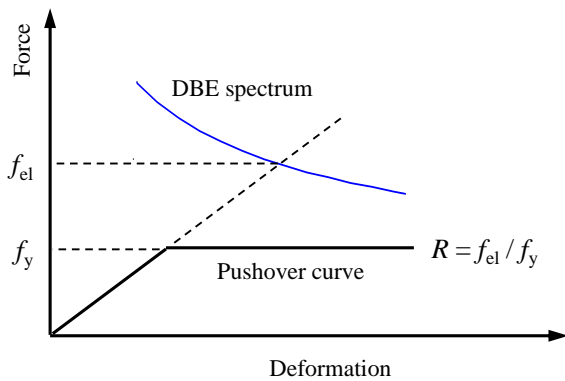


Fig. 5 Definition of strength reduction factor, R

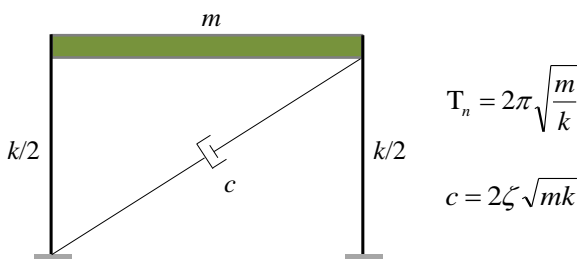


Fig. 6 Schematic of the SDOF systems

## 6. SDOF results

The seismic performance upon a representative earthquake ground motion record is examined firstly. In this case, record LA19 is selected, due to the corresponding spectra acceleration well matches that on the design spectrum at this specific fundamental period. Fig. 7 plots the time histories of four seismic response indices. Time duration is truncated at 40 seconds, since the structural vibrations have already come to rest.

As shown in Fig. 7(a), the peak deformations are reached at different times depending on the temperature. They are 13.3, 11.5, 13.0, 14.0 and 15.8 cm at the temperatures of  $-40$ ,  $-20$ ,  $0$ ,  $20$  and  $40^\circ\text{C}$ , respectively. The displacement demands exhibit a maximum difference of 21% when the temperature deviates from the reference state by  $\pm 40^\circ\text{C}$ . It is interesting to note that the disparity in deformation demands is small, compared to the difference in the hysteretic behavior of systems. This can be understood by combining the variation trends of strength and equivalent damping ratio. As can be seen in Table 1, the temperature variation leads to contrast trends on strength and equivalent damping ratio. Therefore, although SMAs at low temperature have a small strength capacity, their damping behavior is enhanced. The competing effects generate minor influence on the deformations. At the end of earthquake, residual deformations are constantly zero under all temperatures, due to the intrinsic recentering behavior.

In terms of acceleration demands, as shown in Fig. 7(b), it is clear that high temperatures lead to larger demand than low temperatures do. The increased acceleration demands are essentially attributed to the larger force demands generated in the systems with higher 'yield' strength induced by the elevated temperature. Parenthetically, it is interesting to note the flat excursions during vibrations, which last for approximately 0.3s. This is caused by the 'yield' behavior. When the systems are deformed into the 'post-yield' branch, the acceleration demands ascend at a low rate, compared to that in the elastic state. Thus, acceleration demand is more sensitive to temperature variation, compared to deformation demand.

The energy performance is assessed as well, as shown in Fig. 7(c) and 7(d). The absorbed energy increases drastically when the structures are deformed into nonlinear state. At high temperatures, the absorbed energy is higher than that at low temperatures during initial responses, but the disparity almost diminishes at the end of vibrations. Regarding the input energy, the demand shows a constantly ascending trend globally. The temperature variation seems remarkably affects the input energy. The input energy approximately doubled when the temperature is increased from  $-40$  to  $40^\circ\text{C}$ . The effect of temperature variation on the absorbed energy and input energy seems different. The disparity is actually primarily attributed to the energy dissipated by the inherent damping behavior. However, the observation of seismic energy from this single case is not general, as will be seen by analyzing all response results.

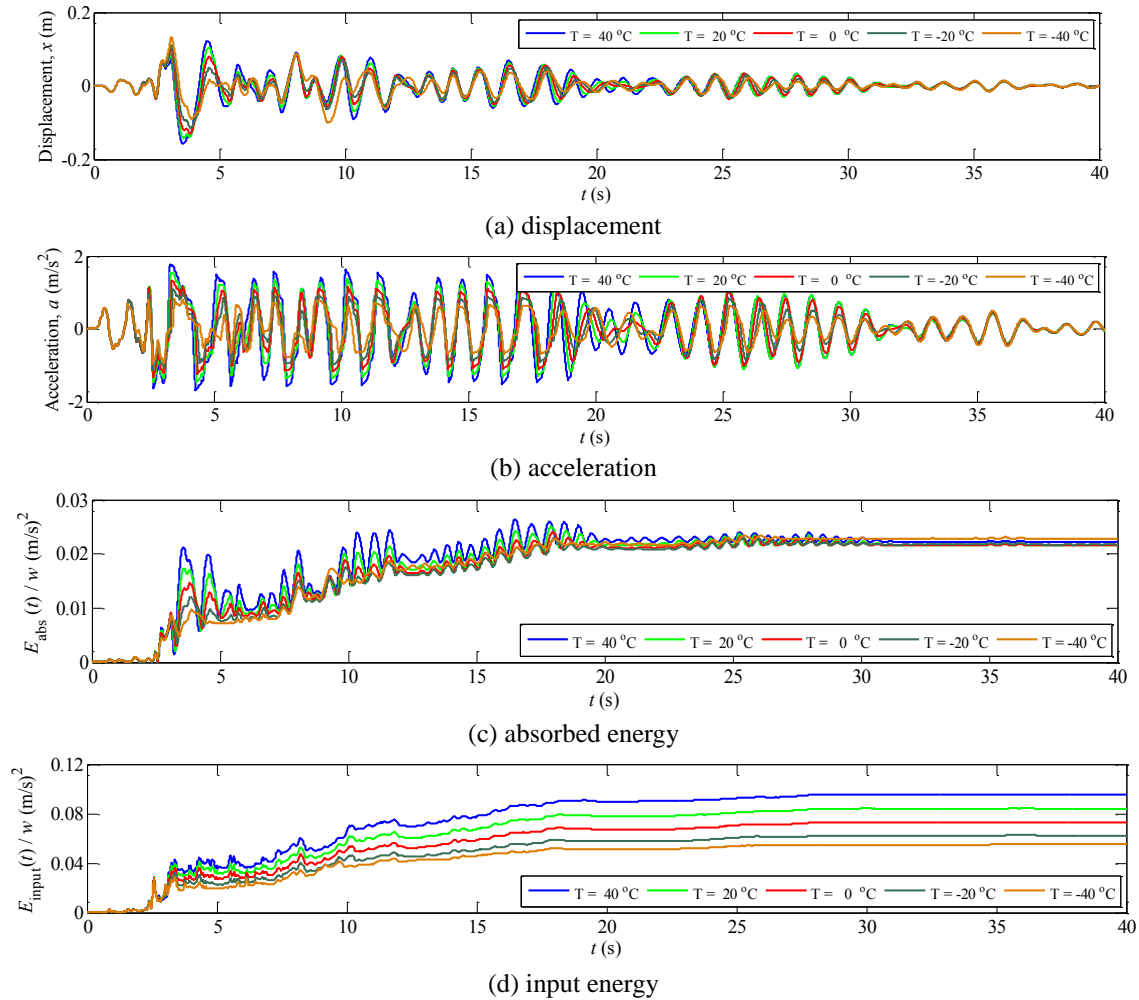


Fig. 7 Time histories of seismic responses upon earthquake ground motion record LA19.  $T_n = 1.1$ s,  $R = 4$

Fig. 8 plots the cyclic behaviors of the systems at various temperatures. The relationships between the displacement and normalized base shear are built. In the positive direction, the displacement demand decreases with the decrease of temperature, whereas, in the negative direction, it tends to show an opposite trend. Thus, the peak displacement seems to show a weak correlation with the temperature variation. The assessment of the time histories of peak displacements, shown in Fig. 7(a), has already confirmed this phenomenon. But it is clear-cut that the systems generate noticeably larger force when the ambient temperature is increased, which is directly induced by the high strength capacity of SMAs at high temperature.

Fig. 9 assembles all the analytical data from the seismic analyses on SDOF systems, and present the results as a function of temperature. Significant deviations can be found between every individual case, caused by the uncertainty nature of earthquakes. To make a straightforward comparison, the mean responses are also given at the top of results corresponding to each specific temperature. Thus the comparisons are based on the mean responses. Compared to that at reference temperature, the deformation demand changes slightly with temperature variation. For example, a decrease of 40°C slightly generates larger deformation by

approximately 4%. But the acceleration demand is noticeably sensitive to temperature variation, compared to the other three performance indices. When the temperature deviates from the reference state for 40°C, the acceleration demand varies by approximately 30%. The acceleration demand changes positively with the variation of temperature, i.e., high temperature leads to large acceleration demand, and vice versa. In addition, the relationship between the variations of acceleration and temperature seems fairly constant across the considered temperature range.

In terms of the absorbed and input energy, the degree of variation is slight. It is seen that SMAs tend to absorb more energy slightly at low temperature, which is primarily attributed to their high damping mechanism at low temperature. For example, compared to the absorbed energy at the highest temperature, the absorbed energy is approximately 28% and 38% higher at 0 and -40°C, respectively. Regarding the input energy, the maximum and minimum values occur at the temperatures of 0 and -40°C, respectively. This response index is relatively stable and shows an unclear trend as the temperature is changing.

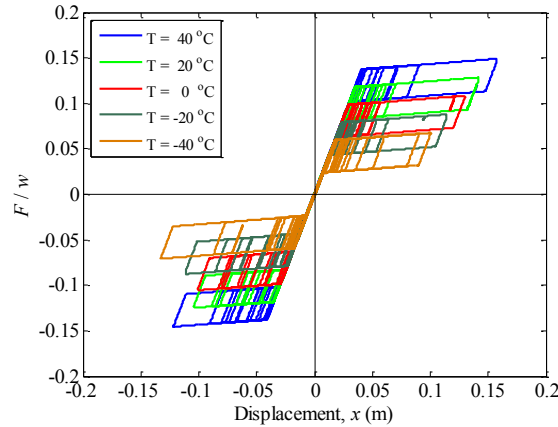


Fig. 8 Cyclic behaviors of the SMA-based SDOF systems upon earthquake ground motion record LA19

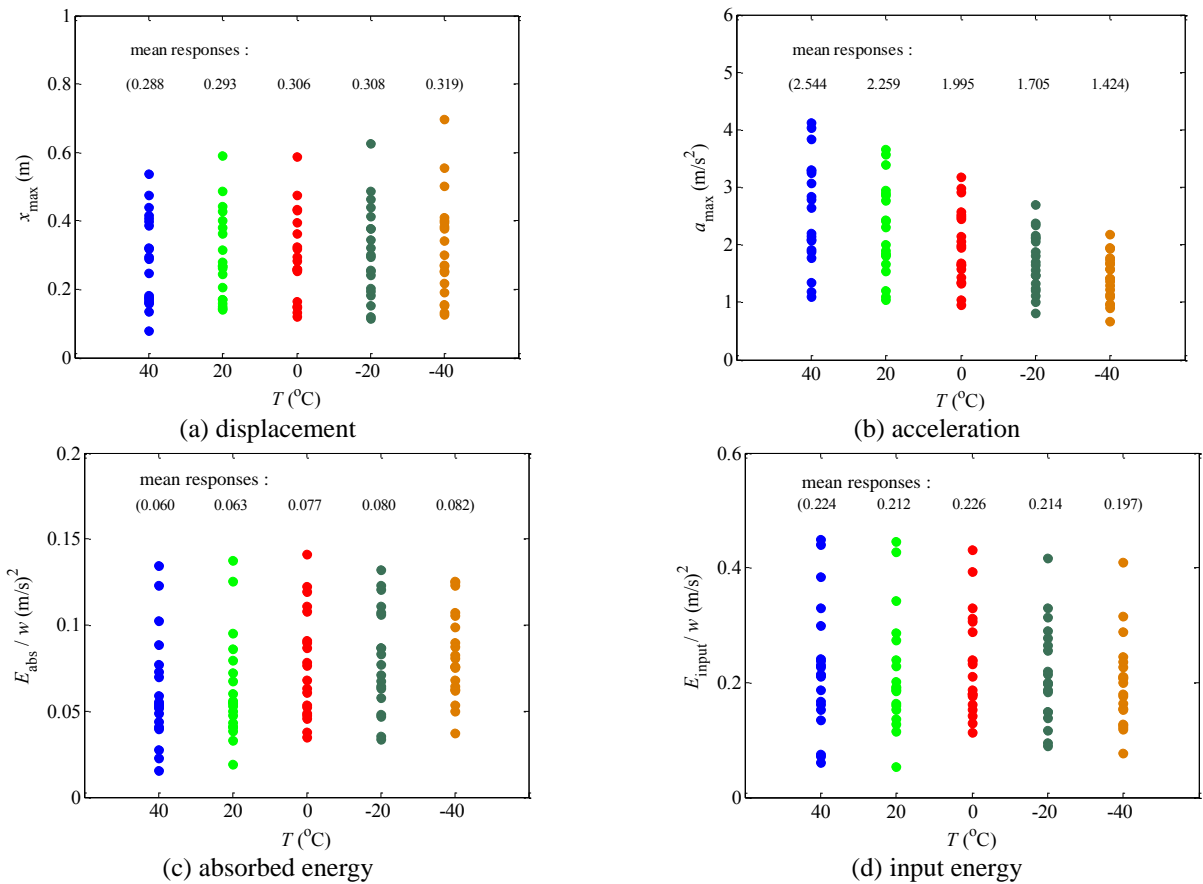


Fig. 9 Assemblage of discrete and mean seismic responses as a function of temperature for SDOF systems

### 7. SMABF

The conclusions based on SDOF analyses are further examined by conducting seismic analysis on a multistory SMABF. According to NEHRP (FEMA 1997), Sabelli *et al.* (2003) designed several multi-story BRBFs which were located in downtown Los Angeles. Among the frames, the six-story frame was adopted, as shown in Fig. 10. The frame has a bay width of 9.14 m, and the story height is 5.49 m for the first story and 3.96 m for the other stories.

This frame has been widely utilized in previous studies (Zhu and Zhang 2008, Qiu *et al.* 2018a, Qiu *et al.* 2018b, Qiu *et al.* 2017). Details of building information can be found in the corresponding study (Sabelli *et al.* 2003). With the same purpose as described in prior studies (Qiu and Zhu 2016), all the beam-to-column connections are modified into pinned joints, which helps to accommodate heavier rotation demand at the connection regions and to isolate the influence from frame mechanism.

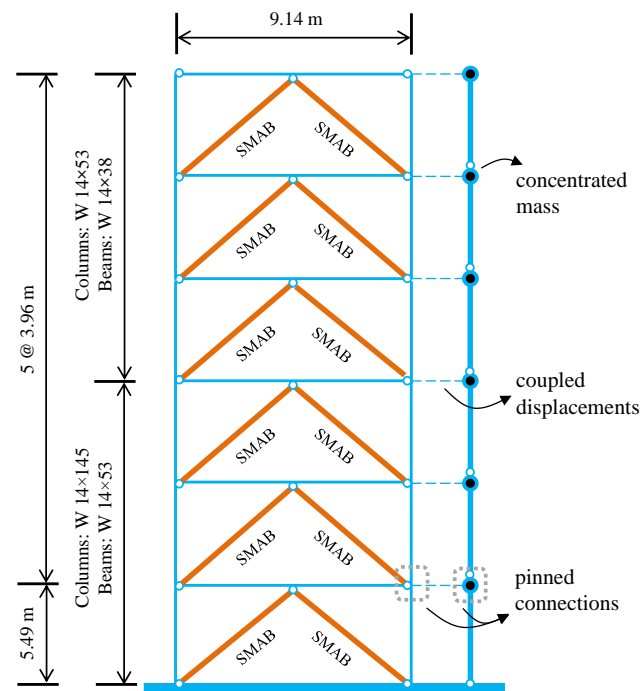


Fig. 10 Elevation view and OpenSees model of the six-story SMABF

Table 2 Design parameters for the SMABF

Parameters		values
Reference temperature, °C		0
Building height, $m$		25.29
Estimated fundamental period, $T$ (s)		1.16
Target interstory drift ratio, $\theta_{IR}$ (%)		1.5
'Yield' interstory drift ratio, $\theta_y$ (%)		0.3
Plastic interstory drift ratio, $\theta_p$ (%)		1.2
Ductility of SMAB		5
Spectral acceleration, $S_d$ (g)		0.61
SMA	$E_A$ , GPa	17.0
	$\sigma_{Ms}$ , MPa	139.0
	$\epsilon_{Ms}$ , %	0.82
	$\alpha$	0.03
	$\beta$	0.36

The sizes of structural components, including the SMABs, beams and columns were determined through a previously developed design methodology (Qiu *et al.* 2017). Since 0 °C is designated to be the reference temperature in current design procedure, the hysteretic properties of SMAs that corresponding to this temperature are taken. The design parameters are listed in Table 2. The performance target is set to be a peak interstory drift ratio of 1.5% upon considered earthquake ground motions, which is consistent with prior studies (Hou *et al.* 2017, Qiu *et al.* 2017). It is noted that the current purpose is to evaluate the effect of temperature variation, so different performance targets can be prescribed as well and the analyses are expected to arrive at consistent conclusions. The 'yield' interstory drift ratio is

defined to be 0.3%, which leads to a plastic interstory drift ratio of 1.2% and a ductility demand of 5 for the SMABs. As mentioned in the part introducing the cyclic behavior of monocrystalline CuAlBe, the deformation within 11% strain can be considered. So the ductility of the SMA should be smaller than the threshold. The fundamental period is estimated to be 1.16s through the inelastic displacement spectrum (Priestley and Kowalsky 2000). The lateral force pattern which considers the high-mode effect (Qiu and Zhu 2016) is adopted to distribute the design base shear to each story. The final fundamental period of the numerical model is 1.1s, which agrees very well with the estimated value.

Table 3 Design results of the SMABF

Members	Story	'Yield' strength, kN	Elastic stiffness, kN/mm
SMABs	1st	1385.2	131.5
	2nd	1121.7	124.9
	3rd	1030.6	114.7
	4th	896.0	99.7
	5th	709.7	79.0
	6th	452.5	50.4
Columns	1st–3rd	W 14×145	
	4th–6th	W 14×53	
Beams	1st–3rd	W 14×53	
	4th–6th	W 14×38	

Table 4 Quantities of SMAs used in each story

Story No.	Cross-sectional area (mm <sup>2</sup> )	Length (m)	Volume (cm <sup>3</sup> )
6	6511.3	1.1	7133.1
5	10212.1	1.1	11187.3
4	12891.8	1.1	14122.8
3	14828.7	1.1	16244.8
2	16140.0	1.1	17681.3
1	19930.3	1.3	25610.3

Table 3 lists the design results, including the capacities of SMABs and the sections of beams and columns. The braces at lower stories show higher strength and stiffness than that at upper stories, since story shear is transferred from top to bottom. In practice, large size wires or cables or bars are suggested to better provide sufficient force and stiffness capacity. The introduced pinned joints release moment constraint, thus the columns and beams sustain axial force only. The cross sectional area are determined by capacity design, with the performance target of maintaining elastic upon considered earthquakes. The sections are selected from available section types to best meet the area requirement. The quantities of SMAs used in each story, including cross-sectional area, length and volume, are listed in Table 4. It is worth noting that it is not reasonable to grow a very large single crystal. As stated previously, the monocrystalline CuAlBe SMA wires are wrapped on the steel rods, so the totally required cross-sectional area of SMAs can be conveniently increased by wrapping sufficient cycles of wires.

## 8. Numerical model

The numerical model was built in seismic simulation platform OpenSees (Mckenna and Fenves 2013). Due to symmetrical plan layout, only one braced bay is modeled, as shown in Fig. 10. The beams and columns are modeled with force-based beam-column elements, as suggested by (Qiu *et al.* 2017). The columns are fixed at their bases, and are continuously modeled with one element in each story. Each beam consists of two elements and jointly connects with the braces at the middle span. Strength and stiffness deterioration of steel material are not considered for the beams and columns. The frame elements use ASTM A992 steel and are modeled by the *Steel02* material. Each brace is

modeled by only one single element, since the braces sustain axial force without buckling. The cross section of the braces at each integration point is an assembly of uniaxial fibers. The *SelfCentering* material, which is essentially a FS hysteresis model, is used to simulate the cyclic behavior of SMABs. But the fatigue behavior of SMAs, as reported by associated studies (Carreras *et al.* 2011, Casciati and Marzi 2010, Casciati and Marzi 2011, Casciati *et al.* 2017), cannot be considered currently by the simulation platform. The tributary floor mass is concentrated on one adjacent leaning column to generate earthquake-induced inertia force. The leaning column is coupled to the frame at each floor level to undergo the same displacements in both horizontal and vertical directions. The coupled displacement are also responsible for generating the *P-Δ* effect during the seismic responses. To exclude the influences from the continuous leaning column (Ji *et al.* 2009, Qu *et al.* 2014, Qu *et al.* 2015), the two adjacent segments are connected by a hinge. Additional time was added at the end of each earthquake ground motion record to damp out the vibrations and to accurately measure residual deformation at the end of responses.

## 9. Nonlinear static behavior

The effect of temperature variation on the global behavior of SMABFs is assessed by conducting nonlinear static analysis, i.e., pushover analysis (Krawinkler and Seneviratna 1998). Before applying the lateral forces to the frames, gravity force was gradually loaded on the numerical model to generate the *P-Δ* effect. The applied lateral force pattern was consistent with the first vibration mode and was maintained throughout the loading procedure. The magnitude of target displacement was set to be corresponding to a roof drift of 2.0%, with a control node at

the roof level. Cyclic loadings were applied to produce the hysteresis loops of structural systems.

Fig. 11 plots the relationships between the normalized base shear and roof drift ratio for the structure at the considered temperatures. It is seen that the base shear demand increases linearly with the increase of environmental temperature, whereas the hysteresis width is almost unaffected. So the equivalent damping ratio tends to decrease at an approximately equal rate as the strength capacity upon the targeted roof drift. The pushover results also imply that the structural behavior is dominated by the properties of SMABs as expected. Therefore, consistent with the effect of temperature variation on the cyclic behavior of the kernel material, i.e., the monocrystalline CuAlBe SMA, the corresponding effect on the structural performance tracks an identical trend.

## 10. Nonlinear dynamic behavior

The static analysis reveals the effect of temperature variation on the global behavior of SMABFs, and shows that the SMABFs perform in different behaviors when the ambient temperature changes. However, their dynamic behaviors upon earthquakes are still unknown and require further investigations. As such, a total of twenty earthquake ground motion records representing the DBE seismic hazard level are input into the SMABFs at various temperatures.

### 10.1 Time history response

The time history analysis was carried out by a case study for demonstration purpose. This case study aims to unveil some general dynamic characteristics of the considered structures induced by different environmental temperatures. To this end, the ground motion record LA19 is selected again, due to its spectral acceleration well matches the design spectrum at the fundamental period of the structure.

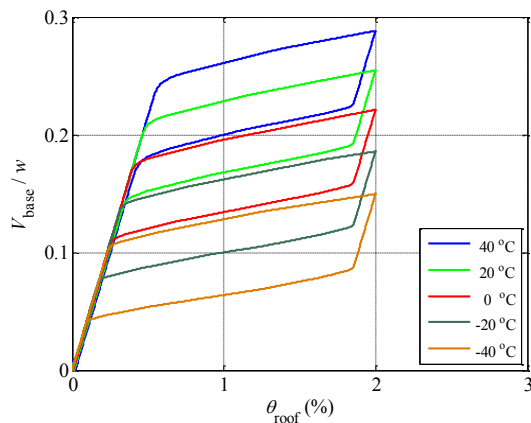


Fig. 11 Nonlinear static behavior of the SMABF under various temperatures

Fig. 12 plots the time histories of roof drift ratios and roof accelerations upon this specific ground motion. The time history curves overlap each other in the initial two seconds and later twenty seconds, because these buildings are vibrating elastically, which is thus not affected by temperature variation. As shown in Fig. 12(a), the peak deformations are reached at almost the same time with nearly identical magnitude, regardless of temperature. The comparisons between roof drift behaviors are well consistent with those between SDOF systems, since the global deformation demand of multi-story frames is usually dominated by the fundamental vibration mode (Newmark 1959). In terms of roof accelerations shown by Fig. 12(b), it is clear that the curves associated with low temperatures are enclosed by those at high temperatures, during the severe nonlinear oscillation process. Particularly, in almost each wave, the temperatures of 40 and  $-40$  °C lead to the largest and smallest accelerations, which indicates that the increase of temperature tends to raise the acceleration demand.

To further investigate the temperature effect on the frame systems from the component level, Fig. 13 plots the cyclic behaviors of the 2nd-story SMABs upon ground motion record LA19. These braces are selected, due to they produce larger deformation demands than those belong to the other stories. It is seen that the braces sustain comparable deformation, even though the temperature deviates from the reference state by  $\pm 40$  °C. The force level noticeably increases with the increase of temperature, attributed to the temperature sensitivity of the SMA.

### 10.2 Peak interstory drift ratio

The peak interstory drift ratios over building height,  $\theta_{\text{peak}}$ , which is closely related to seismic damage, is assessed. Considering the seismic response is significantly record-dependent, only the mean values are plotted to represent the central tendency of responses upon the considered suite of ground motion records. Fig. 14 assembles the  $\theta_{\text{peak}}$  at various temperatures and the performance target prescribed in the design procedure of SMABF at 0 °C. It is seen that the designed structure, i.e., the structure at 0 °C, meets the target very well over the entire building height except for the first story. The relatively small deformation at the first story is attributed to resistance contribution by rigid column bases. More importantly, regardless of temperature varying, the structures almost perform identically in every single story. Therefore, the investigation into the peak interstory drift ratio indicates that the temperature variation generates minor effect on the seismic deformation demand of SMABFs.

### 10.3 Peak floor acceleration

Besides with the peak deformation demand, the peak acceleration demands over building height,  $A_{\text{peak}}$ , is also analyzed, as shown in Fig. 15. The analyses on  $A_{\text{peak}}$  particularly shed light on the damage risk of non-structural components. Similar to the  $\theta_{\text{peak}}$ , only the mean values of  $A_{\text{peak}}$  are plotted for this comparison. The performance target is not included, since the adopted design approach is

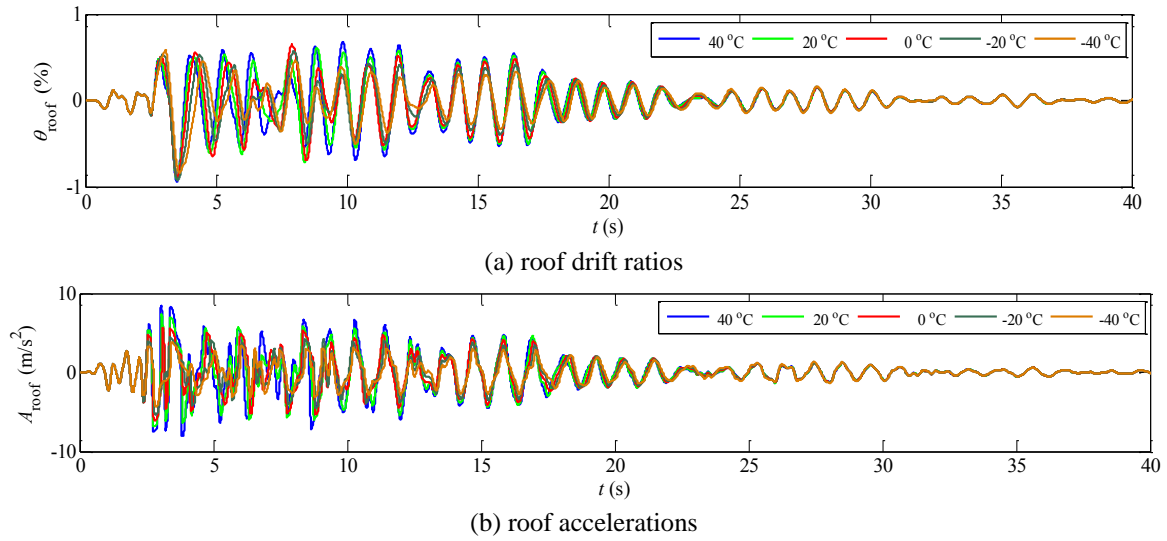


Fig. 12 Time history upon earthquake ground motion record LA19

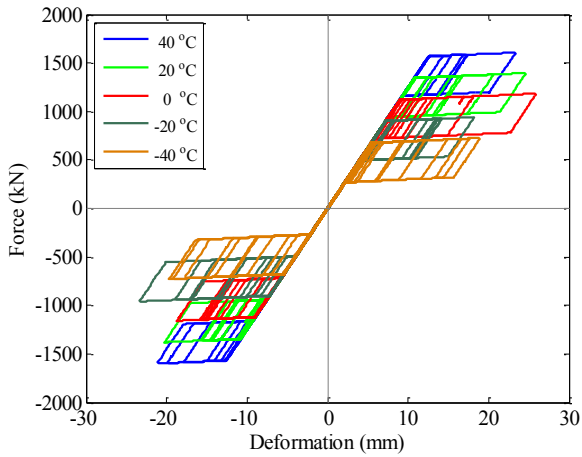


Fig. 13 Cyclic behaviors of the 2nd-story SMABs upon earthquake ground motion record LA19

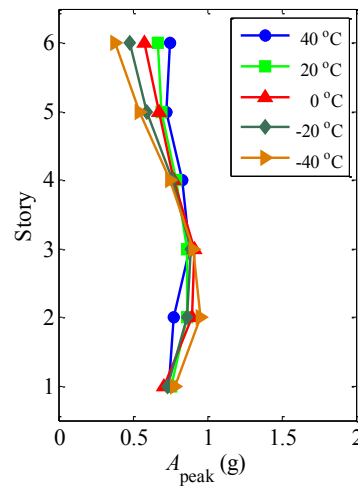


Fig. 15 Peak floor accelerations over building height

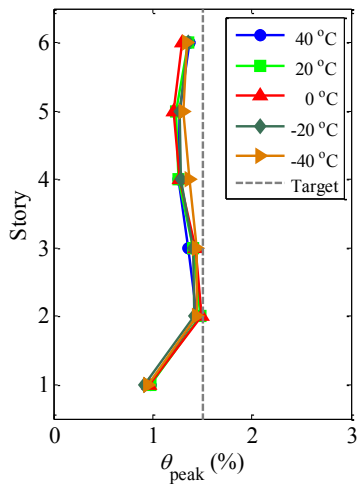


Fig. 14 Peak interstory drift ratios over building height

displacement oriented. It is seen that the values of  $A_{peak}$  are comparable in the low-to-middle stories among the considered temperatures. However, at the 5th and 6th stories,  $A_{peak}$  decreases with the decrease of temperature. Particularly, the  $A_{peak}$  at the 6th story reduced gradually from 0.75 to 0.38 g with a decrement of approximately  $0.05 (m/s^2) / ^\circ C$ , when the temperature is decreased from 40 to  $-40^\circ C$ . The effect of temperature variation on the global acceleration demands of the multi-story frame shows a similar trend as that of the SDOF systems, and can be interpreted from the perspective of equivalent damping ratio as well.

#### 10.4 Residual interstory drift ratio

The residual interstory drift ratios over building height,  $\theta_r$ , is a critical seismic performance index, which defines the post-event state of structures. Excessive residual

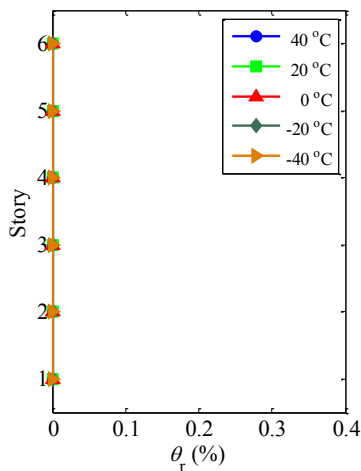


Fig. 16 Residual interstory drift ratios over building height

deformation deteriorates the structural earthquake resilience, although this index was not explicitly considered in the design procedure. Fig. 16 plots the mean values of  $\theta_r$  for the frame structure at different temperatures. It is shown that the residual interstory drift ratios are constantly zero in each story even if the temperature is down to  $-40^\circ\text{C}$ . The structure under all temperatures shows zero residual deformation, attributed to the well maintained superelasticity of SMAs within the considered temperature range. This analysis indicates that the SMABF is able to return to the at-rest position and stand exactly vertically at the end of the motion, as long as the SMAs maintain superelasticity.

## 11. Conclusions

In this study, the effect of temperature variation on the seismic behavior of SMABFs is examined numerically. The considered temperatures are from  $-40$  to  $40^\circ\text{C}$  with an interval of  $20^\circ\text{C}$ . The current SMAB utilizes superelastic monocrySTALLINE CuAlBe cables that exhibit superelastic behavior within the interested temperature range. The seismic analyses on SDOF systems and a multi-story SMABF are conducted by subjecting the systems to a suite of earthquake ground motions corresponding to the DBE hazard level. Following conclusions can be obtained:

- The seismic performance indices, including peak deformation, absorbed energy and input energy, of SMA-based SDOF systems show minor sensitivity to the temperature variation.
- The deformation demand of the SMABF is almost not affected by the change of environmental temperature. Therefore, although the frame structure was designed by assuming an operating temperature of  $0^\circ\text{C}$ , it constantly shows satisfactory seismic performance and always meets the prescribed performance target, regardless of temperature variations.

- For the SDOF systems and SMABF, both of their acceleration demands are sensitive to temperature variation, showing a noticeable increase with the increase of temperature. Particularly, when the environmental temperature is elevated, the roof acceleration of SMABF will be increased at a rate of  $0.05 \text{ (m/s}^2\text{) / }^\circ\text{C}$ .

- Due to the selected SMA exhibits superelasticity within the interested temperature range, the SMABF always leaves zero residual deformation after earthquakes even the temperature is down to  $-40^\circ\text{C}$ . The analytical results indicated the monocrySTALLINE CuAlBe is particularly appealing in low-temperature environment, which is greatly attributed to the effect of the low coefficient of temperature and the stresses achievable without plastic deformation.

- Considering SDOF systems generally represent the global behavior of the corresponding MDOF systems, the current findings also shed light on the other types of structural systems equipped with SMA-based devices.

However, it is worth noting that the above conclusions are based on the premise that the selected SMA should well maintain superelasticity under the considered temperatures. If the SMAs those start to lose superelasticity at low temperature are utilized, the conclusions from this study may be no longer accurate to a certain degree. As such, further investigation is required to address the effect of temperature variation on the seismic behavior of structures with different SMA-based components.

## Acknowledgements

This research was supported by the National Natural Science Foundation of China (No.: 51808317), the Natural Science Foundation of Shandong Province, China (No.: ZR2017BEE004), and the China Postdoctoral Science Foundation (No.: 2017M622206). However, any opinions, findings, conclusions and recommendations presented in this paper are those of the authors and do not necessarily reflect the views of the sponsors. Finally yet importantly, the authors wish to thank the anonymous reviewers for their careful evaluations and insightful comments that helped improve the paper.

## References

- Andrawes, B. and DesRoches, R. (2007), "Effect of ambient temperature on the hinge opening in bridges with shape memory alloy seismic restrainers", *Eng. Struct.*, **29**(9), 2294-2301.
- Araki, Y., Endo, T., Omori, T., Sutou, Y., Koetaka, Y., Kainuma, R. and Ishida K. (2011), "Potential of superelastic Cu-Al-Mn alloy bars for seismic applications", *Earthq. Eng. Struct. D.*, **40**(1), 107-115.
- Carreras, G., Casciati, F., Casciati, S., Isalgue, A., Marzi, A. and Torra, V. (2011), "Fatigue laboratory tests toward the design of SMA portico-braces", *Smart Struct. Syst.*, **7**(1), 41-57.
- Casciati, F. and Faravelli, L. (2009), "A passive control device

- with SMA components from the prototype to the model”, *Struct. Control. Health. Monit.*, **16**(7-8), 751-765.
- Casciati, S., Faravelli, L. and Vece, M. (2017), “Investigation on the fatigue performance of Ni-Ti thin wires”, *Struct. Control Health Monit.*, **24**, e1855. doi: 10.1002/stc.1855.
- Casciati, S. and Marzi, A. (2010), “Experimental studies on the fatigue life of shape memory alloy bars”, *Smart Struct. Syst.*, **6**(1), 73-85.
- Casciati, S. and Marzi, A. (2011), “Fatigue tests on SMA bars in span control”, *Eng. Struct.*, **33**(33), 1232-1239.
- Chang, K.C., Soong, T.T., Oh, S.T. and Lai, M.L. (1992), “Effect of ambient temperature on viscoelastically damped structure”, *J. Struct. Eng. - ASCE*, **118**(7), 1955-1973.
- Chang, K.C., Soong, T.T., Oh, S.T. and Lai, M.L. (1995), “Seismic behavior of steel frame with added viscoelastic dampers”, *J. Struct. Eng. - ASCE*, **121**(10), 1418-1426.
- Chopra, A.K. (1995), *Dynamics of Structures: Theory and Applications to Earthquake Engineering*, Prentice-Hall: Englewood Cliffs, NJ.
- Chopra, A.K. and Goel, R.K. (2002), “A modal pushover analysis procedure for estimating seismic demands for buildings”, *Earthq. Eng. Struct. D.*, **31**(3), 561-582.
- de Castro Bubani, F., Sade, M., Torra, V., Lovey, F. and Yawny, A. (2013), “Stress induced martensitic transformations and phases stability in Cu–Al–Be shape-memory single crystals”, *Mater. Sci. Eng.*, **583**, 129-139.
- DesRoches, R. and Smith, B. (2004), “Shape memory alloys in seismic resistant design and retrofit: a critical review of their potential and limitations”, *J. Earthq. Eng.*, **8**(3), 415-429.
- Fahnestock, L.A., Ricles, J.M. and Sause R. (2007), “Experimental evaluation of a large-scale buckling-restrained braced frame”, *J. Struct. Eng. - ASCE*, **133**(9), 1205-1214.
- Fang, C., Yam MCH, Lam ACC and Xie, LK. (2016), “Cyclic performance of extended end-plate connections equipped with shape memory alloy bolts”, *J. Constr. Steel Res.*, **94**, 122-136.
- FEMA (1997), *NEHRP Recommended provisions for seismic regulations for new buildings and other structures*, Federal Emergency Management Agency, Washington, DC.
- Guo, W.W., Daniel, Y., Montgomery, M. and Christopoulos, C. (2016), “Thermal-mechanical model for predicting the wind and seismic response of viscoelastic dampers”, *J. Eng. Mech. - ASCE*, **142**(10), 04016067.
- Hou, H., Li, H., Qiu, C. and Zhang, Y. (2017), “Effect of hysteretic properties of SMAs on seismic behavior of self-centering concentrically braced frames”, *Struct. Control Health Monit.*, <https://doi.org/10.1002/stc.2110>.
- Ji, X., Kato, M., Wang, T., Hitaka, T. and Nakashima, M. (2009), “Effect of gravity columns on mitigation of story drift concentration for concentrically braced steel frames”, *J. Constr. Steel Res.*, **65**(12), 2148-2156.
- Katariya P.V., Panda, S.K., Hirwani C.K., Mehar K. and Thakare O. (2017), “Enhancement of thermal buckling strength of laminated sandwich composite panel structure embedded with shape memory alloy fibre”, *Smart Struct. Syst.*, **20**(5), 595-605.
- Kiggins, S. and Uang, C.M. (2006), “Reducing residual drift of buckling-restrained braced frames as a dual system”, *Eng. Struct.*, **28**(11), 1525-1532.
- Krawinkler, H. and Seneviratna, G. (1998), “Pros and cons of a pushover analysis of seismic performance evaluation”, *Eng. Struct.*, **20**, 452-464.
- Liu, J.L., Zhu, S., Xu, Y.L. and Zhang, Y.F. (2011), “Displacement-based design approach for highway bridges with SMA isolators”, *Smart Struct. Syst.*, **8**(2), 173-190.
- MathWorks, MATLAB — The Language of Technical Computing, Version 2011a. (2011), MathWorks, Natick, MA.
- McCormick, J., Aburano, H., Ikenaga, M. and Nakashima, M. (2008), “Permissible residual deformation levels for building structures considering both safety and human elements”, *Proceedings of the 14th World Conference on Earthquake Engineering, Beijing, China*, Paper No. 05-06-0071.
- McCormick, J., DesRoches, R., Fugazza, D. and Auricchio, F. (2007), “Seismic assessment of concentrically braced steel frames with shape memory alloy braces”, *J. Struct. Eng. - ASCE*, **133**(6), 862-870.
- Mckenna, F. and Fenves, G.L. (2013), Open system for earthquake engineering simulation (OpenSees), *Pacific earthquake engineering research center. University of California*.
- Moehle, J.P. (1992), “Displacement-based design of RC structures subjected to earthquakes”, *Earthq. Spectra*, **8**(3), 403-428.
- Newmark, N.M. (1959), “A method of computation for structural dynamics”, *J. Eng. Mech. Div.*, **85**(3), 67-94.
- Ozbulut, O.E. and Hurlbaeus, S. (2010), “Evaluation of the performance of a sliding-type base isolation system with a NiTi shape memory alloy device considering temperature effects”, *Eng. Struct.*, **32**(1), 238-249.
- Ozbulut, O.E. and Hurlbaeus, S. (2012), “Application of an SMA-based hybrid control device to 20-story nonlinear benchmark building”, *Earthq. Eng. Struct. D.*, **41**(13), 1831-1843.
- Ozbulut, O.E., Hurlbaeus, S. and DesRoches, R. (2011), “Seismic response control using shape memory alloys, a review”, *J. Intel. Mat. Syst. Str.*, **22**(14), 1531-1549.
- Ozbulut, O.E. and Silwal B. (2016), “Performance assessment of buildings isolated with S-FBI system under near-fault earthquakes”, *Smart Struct. Syst.*, **17**(5), 709-724.
- Park J.K. and Park S. (2016), “Intelligent bolt-jointed system integrating piezoelectric sensors with shape memory alloys”, *Smart Struct. Syst.*, **17**(1), 135-147.
- Priestley, M.J.N. and Kowalsky, M.J. (2000), “Direct displacement-based seismic design of concrete buildings”, *Bull. New Zeal Soc. Earthq. Eng.*, **33**(4), 421-444.
- Qiu, C., Li, H., Ji, K., Hou, H. and Tian, L. (2017), “Performance-based plastic design approach for multi-story self-centering concentrically braced frames using SMA braces”, *Eng. Struct.*, **153**, 628-638.
- Qiu, C., Zhang, Y., Li, H., Qu, B., Hou, H. and Tian, L. (2018a), “Seismic performance of concentrically braced frames with non-buckling braces: a comparative study”, *Eng. Struct.*, **154**, 93-102.
- Qiu, C., Zhang, Y., Qi, J. and Li, H. (2018b), “Seismic behavior of properly designed CBFs equipped with NiTi SMA braces”, *Smart Struct. Syst.*, **21**(4), 479-491.
- Qiu, C. and Zhu, S. (2014), “Characterization of cyclic properties of superelastic monocrystalline Cu–Al–Be SMA wires for seismic applications”, *Constr. Build. Mater.*, **72**, 219-230.
- Qiu, C. and Zhu, S. (2016), “High-mode effects on seismic performance of multi-story self-centering braced steel frames”, *J. Constr. Steel Res.*, **119**, 133-143.
- Qiu, C. and Zhu, S. (2017), “Shake table test and numerical study of self-centering steel frame with SMA braces”, *Earthq. Eng. Struct. D.*, **46**(1), 117-137.
- Qu, B., Sanchez-Zamora, F. and Pollino, M. (2014), “Mitigation of inter-story drift concentration in multi-story steel concentrically braced frames through implementation of rocking cores”, *Eng. Struct.*, **70**(9), 208-217.
- Qu, B., Sanchez-Zamora, F. and Pollino, M. (2015), “Transforming seismic performance of deficient steel concentrically braced frames through implementation of rocking cores”, *J. Struct. Eng. - ASCE*, **141**(5), 04014139.
- Sabelli, R., Mahin, S. and Chang, C. (2003), “Seismic demands on steel braced frame buildings with buckling-restrained braces”, *Eng. Struct.*, **25**(5), 655-666.
- Sade, M., de Castro Bubani, F., Lovey, F.C. and Torra, V. (2014), “Effect of grain size on stress induced martensitic transformations in a Cu–Al–Be polycrystalline shape-memory

- alloy. Pseudoelastic cycling effects and microstructural modifications”, *Mater. Sci. Eng.: A*, **609**, 300-309.
- Sommerville, P., Smith, N.F., Punyamurthula, S. and Sun, J. (1997), *Development of ground motion time histories for Phase 2 of the FEAM/SAC steel project*, SAC Background Document SAC/BD-91/04. Sacramento, Calif.: SAC Joint Venture.
- Song, G., Ma, N. and Li, H.N. (2006), “Applications of shape memory alloys in civil structures”, *Eng. Struct.*, **28**(9), 1266-1274.
- Tsai, C.S. (1994), “Temperature effect of viscoelastic dampers during earthquakes”, *J. Struct. Eng. - ASCE*, **120**(2), 394-409.
- Torra, V., Carreras, G., Casciati, S. and Terriault, P. (2014), “On the NiTi wires in dampers for stayed cables”, *Smart Struct. Syst.*, **13**(3), 353-374.
- Torra, V., Isalgue, A., Martorelli, F., Lovey, F.C. and Terriault, P. (2010), “Damping in Civil Engineering Using SMA. Part I: Particular Properties of CuAlBe for Damping of Family Houses”, *Canadian Metallurgical Quarterly*, **49**(2), 179-190.
- Zhang, Y., Camilleri, J.A. and Zhu, S. (2008), “Mechanical properties of superelastic Cu–Al–Be wires at cold temperatures for the seismic protection of bridges”, *Smart Mater. Struct.*, **17**, 025008.
- Zhang, Y., Hu, X. and Zhu, S. (2010), “Seismic performance of benchmark base-isolated bridges with superelastic Cu–Al–Be restraining damping device”, *Struct. Control Health Monit.*, **16**(6), 668-685.
- Zhu, S. and Zhang, Y. (2008), “Seismic analysis of concentrically braced frame systems with self-centering friction damping braces”, *J. Struct. Eng. - ASCE*, **134**(1), 121-131.
- Zhu, S. and Zhang, Y. (2013), “Loading rate effect on superelastic SMA-based seismic response modification devices”, *Earthq. Struct.*, **4**(6), 607-627.